A NEW HYBRID ALGORITHM FOR SOLVING TRANSIENT COMBINED CONDUCTION RADIATION HEAT TRANSFER PROBLEMS

by

Raoudha CHAABANE*, Faouzi ASKRI, and Sassi Ben NASRALLAH

Laboratoire d'Etudes des Systèmes Thermiques et Energétiques (LESTE),
Ecole Nationale d'Ingénieurs de Monastir, Monastir, Tunisia

Original scientific paper
UDC: 536.24/.25:517.96
DOI: 10.2298/TSCI100722015C

A new algorithm based on the lattice Boltzmann method and the control volume finite element method is proposed as an hybrid solver for two dimensional transient conduction and radiation heat transfer problems in an optically emitting, absorbing and scattering medium. The lattice Boltzman method was used to solve the energy equation and the control volume finite element method was used to compute the radiative information. The advantages of the proposed methodology is to avoid problems that confronted when previous techniques are used to predict radiative heat transfer, essentially, in complex geometries and when there is scattering and/or non-black boundaries surfaces. This method combination, which is applied for the first time to solve this unsteady combined mode of heat transfer, has been found to accurately predict the effects of various thermophysical parameters such as the scattering albedo, the conduction-radiation parameter and the extinction coefficient on temperature distribution. The results of this method combination were found to be in excellent agreement with the lattice Boltzmann/collapsed dimension method this proposed numerical approach include, among others, simple implementation on a computer, accurate CPU time, and capability of stable simulation.

Keywords: *lattice Boltzman method, control volume finite element method, participating medium, coupled conduction-radiation*

Introduction

Over the last decay, the lattice Boltzmann method (LBM) has met with significant success for the numerical simulation of a large variety of problems in science and engineering [1-7]. Traditional computational fluid dynamics (CFD) techniques solve the macroscopic transport equations of fluid flow, mass and heat transfer by directly discretizing them. Common numerical methods for solving the Navier-Stokes equations and the energy equation involve discretization of these non-linear partial differential equations by finite difference methods (FDM), finite volume methods (FVM), *etc*. LBM uses, on the other hand, kinetic equation models and corresponding relations between the actually simulated statistical dynamics at a microscopic level and the transport equations at the macroscopic level. This bottom-up approach of the LBM assures by construction the conservation of the relevant

* Corresponding author; e-mail: raoudhach@gmail.com

macroscopic quantities such as mass and momentum [1-5]. LBM inherits many of the advantages of molecular dynamics and kinetic theories, due to its microscopic origin. But it does not use complicated kinetic equations. In comparison with the conventional CFD methods, the advantages of LBM include simple calculation procedure, simple and efficient implementation for parallel computation, easy and robust handling of complex geometries, and others [1-13]. The LBM is second-order accurate in time and space, which is sufficient for most engineering applications and, provided that boundaries are appropriately treated, makes LBM competitive for complex domain geometries. Literature deals with many applications to the conduction-radiation heat transfer problems, the LBM was found to provide accurate results and compatibilities of the LBM for solution of energy equation and the discrete transfer method (DTM) [14], the collapsed dimension method (CDM) [15], the discrete ordinate method (DOM) [16] and the finite volume method (FVM) [17] for the determination of radiative information were established.

The aim of present study is to establish the compatibility and the performance of the LBM for the solution of the energy equation and the control volume finite element method (CVFEM) [18-20] for the determination of radiative information. To that end, a benchmark problem dealing with transient conduction radiation heat transfer in a 2-D enclosure is considered. The effects of the scattering albedo, the conduction-radiation parameter and the grid size are studied. Results of the LBM-CVFEM and the LBM-CDM are compared against each other. Effects of the spatial and angular resolutions on the results are also reported.

Governing equations

In the absence of convection and heat generation, for a homogeneous medium, the energy equation is given by:

$$\frac{\partial T}{\partial t} = \frac{k}{\rho c_p}\nabla^2 T - \frac{\nabla \vec{q}_R}{\rho c_p} \tag{1a}$$

$$\vec{q}_R = \int_{\Omega=4\pi} I(s,\vec{\Omega})\,\vec{\Omega}\,\mathrm{d}\Omega \tag{1b}$$

where ρ is the density, c_p – the specific heat, k – the thermal conductivity, and $\vec{q}_R$ represents the radiative heat flux.

For the RTE, an absorbing, emitting and scattering grey medium can be written as:

$$\vec{\nabla}[I(s,\vec{\Omega})\vec{\Omega}] = -(k_a + k_d)I(s,\vec{\Omega}) + k_a I_b(s) + \frac{k_d}{4\pi}\int_{\Omega'=4\pi} I(s,\vec{\Omega}')\Phi(\vec{\Omega}'\to\vec{\Omega})\mathrm{d}\Omega' \tag{2}$$

where $I(s,\vec{\Omega})$ is the radiative intensity, which is a function of position s and direction $\vec{\Omega}$, k_a and k_d are absorption and scattering coefficients, respectively; $I_b(s)$ – the blackbody radiative intensity at the temperature of the medium; and Φ – the scattering phase function from the incoming $\vec{\Omega}'$ direction to the outgoing direction $\vec{\Omega}$. The term on the left-hand side represents the gradient of the intensity in the direction $\vec{\Omega}$. The three terms on the right-hand side represent the changes in intensity due to absorption and out-scattering, emission, and in-scattering, respectively.

The radiative boundary condition for eq. (2), when the wall bounding the physical domain is assumed grey and emits and reflects diffusely, can be expressed as:

$$I_{\mathrm{w}}(\vec{\Omega}) = \frac{\varepsilon_{\mathrm{w}}\sigma T_{\mathrm{w}}^4}{\pi} + \frac{1-\varepsilon_{\mathrm{w}}}{\pi} \int_{\vec{\Omega}'\vec{\mathrm{n}}_{\mathrm{w}}<0} I_{\mathrm{w}}(\vec{\Omega}') \left|\vec{\Omega}'\vec{\mathrm{n}}_{\mathrm{w}}\right| \mathrm{d}\Omega' \tag{3}$$

where $\vec{\mathrm{n}}_{\mathrm{w}}$ is the unit normal vector on the wall and ε_{w} represents the wall emissivity.

Numerical resolution of the radiative information

Angular and spatial discretization

In the CVFEM, the spatial and angular domains are divided into a finite number of control volumes and control solid angles, respectively. For angular discretization, the direction of propagation $\vec{\Omega}$ is defined by the couple (θ, φ) where θ and φ arethe polar and azimuthal angles, respectively.The total solid angle is subdivided into $N_\theta \times N_\varphi$ control solid angles as depicted in fig. 1, where $\Delta\varphi = (\varphi^+ - \varphi^-) = 2\pi/N_\varphi$ and $\Delta\theta = \pi/N_\theta$. The N_φ and N_θ, represent numbers of control angles in the polar and azimuthal directions, respectively. These $N_\varphi N_\theta$ control solid angles are non-overlapping, and their sum is 4π. The control solid angle $\Delta\Omega^{mn}$ is given by fig. 1(a):

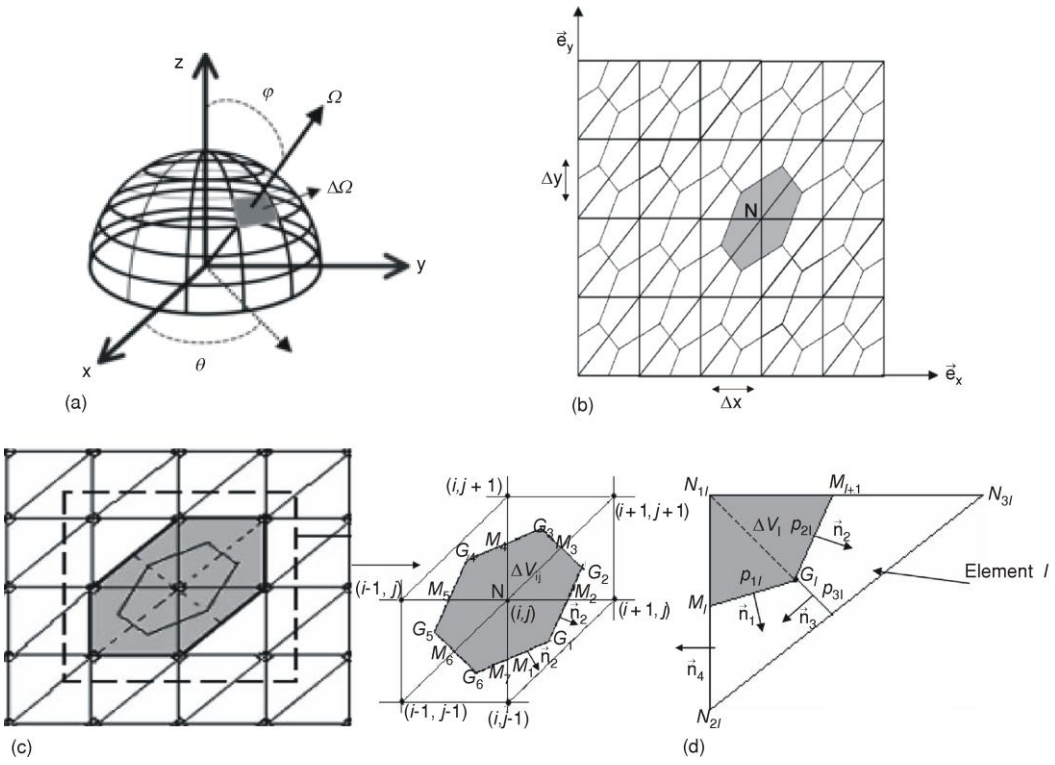

Figure 1. (a) Angular discretization, (b) Spatial discretization in ($\vec{e}_x$, $\vec{e}_y$) plan, (c) Control volume ΔV_{ij}, (d) Subvolume cross-section in ($\vec{e}_x$, $\vec{e}_y$) plan

$$\Delta\Omega^{mn} = \int_{\Delta\theta}\int_{\Delta\phi} \sin\theta \,\mathrm{d}\theta\mathrm{d}\phi \tag{4}$$

For spatial domain is subdivided into three-node triangular elements. As shown in fig. 1(b), a control volume ΔV_{ij} is created around each node N by enjoining the controids G_l of the elements to midpoints M_l and M_{l+1} of the corresponding sides. Each element has two faces, M_lG_l and G_lM_{l+1}; bounding the sub-control volume around N; and each control volume is constructed by adding all subvolumes $NM_lG_lM_{l+1}N$, fig. 1(c). The obtained mesh is composed of N_xN_y control volumes ΔV_{ij}. The N_x and N_y represent numbers of nodes in x and y direction, respectively. Δx and Δy represent the regular steps in x and y-direction, fig. 1(b).

Discretized RTE

Integrating eq. (3) over the control volume ΔV_{ij}, fig. 1(c), and the control solid angle $\Delta\Omega^{mn}$ fig. 1(a), we obtain:

$$\begin{aligned}\int_{A^N}\int_{\Delta\Omega^{mn}} I(s,\vec{\Omega})\vec{\Omega}\vec{n}_N \mathrm{d}\Omega\mathrm{d}A = -\int_{\Delta V_{ij}}\int_{\Delta\Omega^{mn}} (k_\mathrm{a}+k_\mathrm{d})I(s,\vec{\Omega})\mathrm{d}\Omega\mathrm{d}V + \\ + \int_{\Delta V_{ij}}\int_{\Delta\Omega^{mn}} (k_\mathrm{a}+k_\mathrm{d})I(s,\vec{\Omega})\mathrm{d}\Omega\mathrm{d}V + \int_{\Delta V_{ij}}\int_{\Delta\Omega^{mn}} \frac{k_\mathrm{d}}{4\pi}\int_{\Omega'=4\pi} I(s,\vec{\Omega})\Phi(\vec{\Omega}'\to\vec{\Omega})\mathrm{d}\Omega'\mathrm{d}\Omega\mathrm{d}V\end{aligned} \tag{5}$$

where A^N represents the surface of the control volume ΔV_{ij}.

In order to approximate the integrals that represents the extinction; emission and in-scattering contributions, the radiation intensity is considered constant within ΔV_{ij} and $\Delta\Omega^{mn}$ an is evaluated at the centroid of the control volume and at the centre direction of the control solide angle. Then, extinction; emission and in-scattering terms in eq. (5) are, respectively, expressed by the following expressions:

$$-\int_{\Delta V_{ij}}\int_{\Delta\Omega^{mn}} (k_\mathrm{a}+k_\mathrm{d})I(s,\vec{\Omega})\mathrm{d}\Omega\mathrm{d}V = (C_\mathrm{ex}^{mn})_{ij} I_{ij}^{mn} \tag{6a}$$

$$\int_{\Delta V_{ij}}\int_{\Delta\Omega^{mn}} k_\mathrm{a} I_\mathrm{b}(s)\mathrm{d}\Omega\mathrm{d}V = (C_\mathrm{ex}^{mn})_{ij} T_{ij}^4 \tag{6b}$$

$$\int_{\Delta V_{ij}}\int_{\Delta\Omega^{mn}} \frac{k_\mathrm{d}}{4\pi}\int_{\Omega'=4\pi} I(s,\vec{\Omega}')\Phi(\vec{\Omega}'\to\vec{\Omega})\mathrm{d}\Omega'\mathrm{d}\Omega\mathrm{d}V = \sum_{m',n'}^{N_\theta\times N_\phi}[(C_\mathrm{diff}^{mnm'n'})_{ij} I_{ij}^{m'n'}] \tag{6c}$$

where

$$(C_\mathrm{ex}^{mn})_{ij} = -(k_\mathrm{a}+k_\mathrm{d})\Delta\Omega^{mn}\Delta V_{ij} \tag{7a}$$

$$(C_{em}^{mn})_{ij} = \frac{\sigma}{\pi} k_\mathrm{a}\Delta\Omega^{mn}\Delta V_{ij} \tag{7b}$$

$$(C_\mathrm{diff}^{mnm'n'})_{ij} = \frac{k_\mathrm{d}}{4\pi}\Phi^{mnm'n'}\Delta\Omega^{m'n'}\Delta\Omega^{mn}\Delta V_{ij} \tag{7c}$$

where $\Phi^{mnm'n'}$ is the averaged scattering phase function from the control solid angle $\Delta W^{m'n'}$ to the control solid angle $\Delta\Omega^{mn}$. The term on the left-hand side in eq. (5) can be written as:

$$\int_{A^N}\int_{\Delta\Omega^{mn}} I(s,\vec{\Omega})\vec{\Omega}\vec{n}_N \mathrm{d}\Omega \mathrm{d}A = \sum_{l=1}^{6}\int_{A_l^N}\int_{\Delta\Omega^{mn}} I(s,\vec{\Omega})\vec{\Omega}\vec{n}_{lN} \mathrm{d}\Omega \mathrm{d}A \tag{8}$$

The surface A_l^N of a subvolume δV_{lij} is formed by four faces, fig 1(d).

To approximate the integral of the radiative intensity over each of the control volume surfaces (panels) within an element fig. 1(d), the intensity is evaluated at the centroid of the panel and it is assumed to prevail over it. Then eq. (8) becomes:

$$\sum_{l=1}^{6}\int_{A_l^N}\int_{\Delta\Omega^{mn}} I(s,\vec{\Omega})\vec{\Omega}\vec{n}_{lN} d\Omega dA = R_1' + R_1'' \tag{9}$$

where

$$R_1' = \sum_{l=1}^{6}\left[\int_{A_{1l}^N}\int_{\Delta\Omega^{mn}} I(s,\vec{\Omega})\vec{\Omega}\vec{n}_{1lN} d\Omega dA + \int_{A_{2l}^N}\int_{\Delta\Omega^{mn}} I(s,\vec{\Omega})\vec{\Omega}\vec{n}_{1lN} d\Omega dA\right] \tag{10a}$$

$$R_1' = \sum_{l=1}^{6}\left[\int_{A_{4l}^N}\int_{\Delta\Omega^{mn}} I(s,\vec{\Omega})\vec{\Omega}\vec{n}_{4lN} d\Omega dA + \int_{A_{5l}^N}\int_{\Delta\Omega^{mn}} I(s,\vec{\Omega})\vec{\Omega}\vec{n}_{5lN} d\Omega dA\right] \tag{10b}$$

For an internal grid, the integral on faces A_{4l}^N and A_{5l}^N annul themselves since the normals of these surfaces are browsed in the inverse senses for two neighboring elements. Then, R_1'' is set as zero. To evaluate the quantity R_1', the radiative intensity is evaluated at the centre direction of the control solide angle $\Delta\Omega^{mn}$ and at the middle of faces.

$$R_1' = \sum_{l=1}^{6}[I_{p1l}^{mn} A_{1l}^N G_{1lN}^{mn} + I_{p2l}^{mn} A_{2l}^N G_{2lN}^{mn}] \tag{11}$$

where

$$G_{ilN}^{mn} = \int_{\Delta\Omega^{mn}} \vec{\Omega}\vec{n}_{ilN} d\Omega \quad i = 1,2 \tag{12}$$

In order to calculate radiative intensities I_{pil}^{mn}, the skew positive coefficient upwind (SPCU) interpolation scheme [19] is used. For example, the value of the intensity on p_{1l}, fig. 1(d), is expressed as:

$$I_{p1l}^{mn} = f_{1l}^{mn+} I_{p2l}^{mn} + (1 - f_{1l}^{mn+}) I_{N1l}^{mn} \quad \text{when} \quad G_{1lN}^{mn} > 0 \tag{13a}$$

$$I_{p1l}^{mn} = f_{1l}^{mn-} I_{p3l}^{mn} + (1 - f_{1l}^{mn-}) I_{N2l}^{mn} \quad \text{when} \quad G_{1lN}^{mn} < 0 \tag{13b}$$

where

$$f_{1l}^{mn+} = \min.\left[\max.\left(-\frac{G_{2lN}^{mn}}{G_{1lN}^{mn}}, 0\right), 1\right] \tag{14a}$$

$$f_{1l}^{mn-} = \min.\left[\max.\left(-\frac{G_{3lN}^{mn}}{G_{1lN}^{mn}}, 0\right), 1\right] \tag{14b}$$

Using the following functions:

$$W_{klN}^{mn} = \max.\left(\frac{G_{klN}^{mn}}{\left|G_{klN}^{mn}\right|}, 0\right), \quad k = 1,2,3 \tag{15}$$

The intensities I_{p1l}^{mn}, I_{p2l}^{mn} and I_{p3l}^{mn} can be written in the following form:

$$I_{p1l}^{mn} = W_{1lN}^{mn}[f_{1l}^{mn+} I_{p2l}^{mn} + (1 - f_{1l}^{mn+}) I_{N1l}^{mn}] + (1 - W_{1lN}^{mn})[f_{1l}^{mn-} I_{p3l}^{mn} + (1 - f_{1l}^{mn-}) I_{N2l}^{mn}] \tag{16a}$$

$$I_{p2l}^{mn} = W_{2lN}^{mn}[f_{2l}^{mn+} I_{p1l}^{mn} + (1 - f_{2l}^{mn+}) I_{N1l}^{mn}] + (1 - W_{2lN}^{mn})[f_{2l}^{mn-} I_{p3l}^{mn} + (1 - f_{2l}^{mn-}) I_{N3l}^{mn}] \tag{16b}$$

$$I_{p3l}^{mn} = W_{3lN}^{mn}[f_{3l}^{mn+} I_{p2l}^{mn} + (1 - f_{3l}^{mn+}) I_{N3l}^{mn}] + (1 - W_{3lN}^{mn})[f_{3l}^{mn-} I_{p1l}^{mn} + (1 - f_{3l}^{mn-}) I_{N2l}^{mn}] \tag{16c}$$

These equations can be expressed as the following matrix form:

$$I_{p1l}^{mn} = [E_{lN}^{mn}] I_{Nl}^{mn}, \quad l = 1,6 \tag{17}$$

where

$$[E_{lN}^{mn}] = [C_{lN}^{mn}]^{-1} [B_{lN}^{mn}] \tag{18a}$$

$$[C_{lN}^{mn}] = \begin{bmatrix} 1 & -W_{1lN}^{mn} f_{1l}^{mn+} & -(1 - W_{1lN}^{mn}) f_{1l}^{mn-} \\ -W_{2lN}^{mn} f_{2l}^{mn+} & 1 & -(1 - W_{2lN}^{mn}) f_{2l}^{mn-} \\ -(1 - W_{3lN}^{mn}) f_{3l}^{mn-} & -W_{3lN}^{mn} f_{3l}^{mn+} & 1 \end{bmatrix} \tag{18b}$$

$$[B_{lN}^{mn}] = \begin{bmatrix} W_{1lN}^{mn}(1 - f_{1l}^{mn+}) & (1 - W_{1lN}^{mn})(1 - f_{1l}^{mn-}) & 0 \\ W_{2lN}^{mn}(1 - f_{2l}^{mn+}) & 0 & (1 - W_{2lN}^{mn})(1 - f_{2l}^{mn-}) \\ 0 & (1 - W_{3lN}^{mn})(1 - f_{3l}^{mn-}) & W_{3lN}^{mn}(1 - f_{3l}^{mn+}) \end{bmatrix} \tag{18c}$$

$$I_{pl}^{mn} = \begin{pmatrix} I_{p1l}^{mn} \\ I_{p2l}^{mn} \\ I_{p3l}^{mn} \end{pmatrix}, \quad I_{Nl}^{mn} = \begin{pmatrix} I_{N1l}^{mn} \\ I_{N2l}^{mn} \\ I_{N3l}^{mn} \end{pmatrix} \tag{18d}$$

So the amount R_1' can be expressed as

$$R_1' = \sum_{l=1}^{6} \sum_{k=1}^{3} \eta_{klN}^{mn} I_{Nkl}^{mn} \tag{19a}$$

where

$$\eta_{klN}^{mn} = A_{1l}^{N} G_{1lN}^{mn} (E_{lN}^{mn})_{1k} + A_{2l}^{N} G_{2lN}^{mn} (E_{lN}^{mn})_{2k} \tag{19b}$$

Replacing *N* by the superscript *ij* indicated in fig. 1, eq. (19-a) can be written as:

$$R_1' = \gamma_{1ij}^{mn} I_{ij-1}^{mn} + \gamma_{2ij}^{mn} I_{i+1j}^{mn} + \gamma_{3ij}^{mn} I_{i+1j+1}^{mn} + \gamma_{4ij}^{mn} I_{ij+1}^{mn} + \gamma_{5i-1j}^{mn} I_{i+1j}^{mn} + \gamma_{6ij}^{mn} I_{i-1j-1}^{mn} + \gamma_{7ij}^{mn} I_{ij}^{mn} \quad (20)$$

where

$$\gamma_{1ij}^{mn} = \eta_{21ij}^{mn} + \eta_{36ij}^{mn} \quad (21a)$$

$$\gamma_{2ij}^{mn} = \eta_{31ij}^{mn} + \eta_{22ij}^{mn} \quad (21b)$$

$$\gamma_{3ij}^{mn} = \eta_{32ij}^{mn} + \eta_{23ij}^{mn} \quad (21c)$$

$$\gamma_{4ij}^{mn} = \eta_{33ij}^{mn} + \eta_{24ij}^{mn} \quad (21d)$$

$$\gamma_{5ij}^{mn} = \eta_{34ij}^{mn} + \eta_{25ij}^{mn} \quad (21e)$$

$$\gamma_{6ij}^{mn} = \eta_{35ij}^{mn} + \eta_{26ij}^{mn} \quad (21f)$$

$$\gamma_{7ij}^{mn} = \sum_{l=1}^{6} \eta_{1lij}^{mn} \quad (21g)$$

Replacing the different terms of eq. (5) by their developed expressions given by eqs. (6 a)-(6c) and (20), we obtain:

$$\gamma_{1ij}^{mn} I_{ij-1}^{mn} + \gamma_{2ij}^{mn} I_{i+1j}^{mn} + \gamma_{3ij}^{mn} I_{i+1j+1}^{mn} + \\ + \sum_{(m',n')=(1,1)}^{(N_\theta, N_\varphi)} \alpha_{ij}^{mnm'n'} I_{ij}^{m'n'} + \gamma_{4ij}^{mn} I_{ij+1}^{mn} + \gamma_{5ij}^{mn} I_{i-1j}^{mn} + \gamma_{6ij}^{mn} I_{i-1j-1}^{mn} = \beta_{ij}^{mn} \quad (22a)$$

where

$$\alpha_{ij}^{mnm'n'} = \begin{cases} [\gamma_{7ij}^{mn} - (C_{\text{ex}}^{mn})_{ij} - (C_{\text{diff}}^{mnmn})_{ij}] & \text{if} \quad (m',n') = (m,n) \\ -(C_{\text{diff}}^{mnm'n'})_{ij} & \text{if} \quad (m',n') \neq (m,n) \end{cases} \quad (22b)$$

$$\beta_{ij}^{mn} = (C_{em}^{mn})_{ij} T_{ij}^4 \quad (22c)$$

The integration of the RTE, eq. (2), over a boundary control volume ΔV_{ij} and a control solid angle $\Delta\Omega^{mn}$ is calculated using the same strategy adopted for an interior control volume and with taking into account the boundaries wall contribution given by eq. (3). It is clear that in the discretized RTE obtained by CVFEM (eq. (20)), six nodes are used for each calculation point instead of four nodes when FVM is used, and therefore, the accuracy of the numerical resolution process is improved. To solve the algebraic system by a direct method or an iterative method in which all the intensities (I_{ij}^{mn}) are calculated simultaneously after each iteration, the establishment of a matrix system is required.

Matrix formulation

In order to formulate the matrix system of the discretized equations, the radiation intensity I_{ij}^{mn} on point *N* defined by (*i*,*j*) and in direction of propagation (*m*,*n*) will be represented by *I*(*l*) where *l* is expressed in terms of *i*, *j*, *m* and *n* as follow:

$$l = (i-1)N_y N_\theta N_\phi + (j-1)N_\theta N_\phi + (m-1)N_\theta + n \tag{23}$$

So the algebraic eq. (20) can be written in the following matrix form:

$$\zeta I = \lambda \tag{24}$$

where ζ is a square matrix having $(N_x \cdot N_y \cdot N_\theta \cdot N_\varphi)^2$ coefficients which are given by:

$$\zeta_{lk} = \begin{cases} \alpha_{ij}^{mnm'n'} & \text{if} \quad k = k_\alpha \\ \gamma_{1ij}^{mn'} & \text{if} \quad k = k_{\gamma 1} \\ \gamma_{2ij}^{mn'} & \text{if} \quad k = k_{\gamma 2} \\ \gamma_{3ij}^{mn'} & \text{if} \quad k = k_{\gamma 3} \\ \gamma_{4ij}^{mn'} & \text{if} \quad k = k_{\gamma 4} \\ \gamma_{5ij}^{mn'} & \text{if} \quad k = k_{\gamma 5} \\ \gamma_{6ij}^{mn'} & \text{if} \quad k = k_{\gamma 6} \\ 0 & \text{if} \quad \text{not} \end{cases} ; \quad \begin{cases} k_\alpha = (i-1)N_y N_\theta N_\phi + (j-1)N_\theta N_\phi + (m'-1)N_\theta + n' \\ k_{\gamma 1} = (i-1)N_y N_\theta N_\phi + (j-2)N_\theta N_\phi + (m-1)N_\theta + n \\ k_{\gamma 2} = iN_y N_\theta N_\phi + (j-1)N_\theta N_\phi + (m-1)N_\theta + n \\ k_{\gamma 3} = iN_y N_\theta N_\phi + jN_\theta N_\phi + (m-1)N_\theta + n \\ k_{\gamma 4} = (i-1)N_y N_\theta N_\phi + jN_\theta N_\phi + (m-1)N_\theta + n \\ k_{\gamma 5} = (i-2)N_y N_\theta N_\phi + (j-1)N_\theta N_\phi + (m-1)N_\theta + n \\ k_{\gamma 6} = (i-2)N_y N_\theta N_\phi + (j-2)N_\theta N_\phi + (m-1)N_\theta + n \end{cases} \quad l = 1 \ldots N_x N_y N_\theta N_\varphi \tag{25}$$

The term λ which appears in eq. (24) represents the vector that contains the medium and the boundaries emission contributions. The coefficients of this vector are given by:

$$\lambda(l) = \beta_{ij}^{mn} \tag{26}$$

This matrix formulation of the discretized RTE permits the use of many iterative method employed in CFD such as Conjugate Gradient methods, Lanczos method, Jaccobi method.In the present work, the obtained matrix system is solved using the conditioned conjugate gradient squared method (CCGS). Once the intensity distributions are known, radiative information $\nabla \vec{q}_R$ required for the energy equation is computed from

$$\nabla \vec{q}_R = k_a (4\sigma T^4 - \int_{\Omega=4\pi} I(s, \vec{\Omega}) d\Omega \tag{27}$$

LBM for energy equation

In order to solve the energy equation, the BGK (for Bhatnagar, Gross and Krook, [1-13]) lattice Boltzmann scheme is used. The lattice Boltzmann method solves the continuous BGK equation on a regular grid in two steps which are applied iteratively to the whole domain at each time step. So, the starting point of the LBM is the kinetic equation which for a 2-D geometry is given by:

$$\frac{\partial f_i(\vec{r},t)}{\partial \tau} + \vec{c}_i \nabla f_i(\vec{r},t) + \frac{F}{m}\frac{\partial f_i(\vec{r},t)}{\partial \tau} = \omega (f_i^{(0)}(\vec{r},t) - f_i(\vec{r},t)), \quad i = 0,1,..,b \tag{28a}$$

$$\tau = \frac{1}{\omega} = \frac{3k}{\rho c_p c^2} + \frac{\Delta t}{2} \tag{28b}$$

$f_i^{(0)}$ is the equilibrium distribution function, τ is the relaxation time, f_i is the particle distribution function denoting the number of particles at the lattice node $\vec{r}(x, y)$ and time t

moving in direction i with velocity $\vec{c}_i$ along the lattice link $\Delta\vec{r} = \vec{c}_i \Delta t$ connecting the nearest neighbours and b is the number of directions in a lattice through which the information propagates. In the absence of force term and using the single time relaxation model of the BGK approximation, the discrete Boltzmann equation is given by [1-13]

$$\frac{\partial f_i(\vec{r},t)}{\partial t} + \vec{c}_i \nabla f_i(\vec{r},t) = -\frac{1}{\tau}[f_i(\vec{r},t) - f_i^{(0)}(\vec{r},t)], \quad i = 1,2,...b \tag{29}$$

After discretization, eq. (29) can be written as [1-13]

$$f_i(\vec{r} + \vec{c}_i \Delta t, t + \Delta t) = f_i(\vec{r},t) - \frac{\Delta t}{\tau}[f_i(\vec{r},t) - f_i^{(0)}(\vec{r},t)] \tag{30}$$

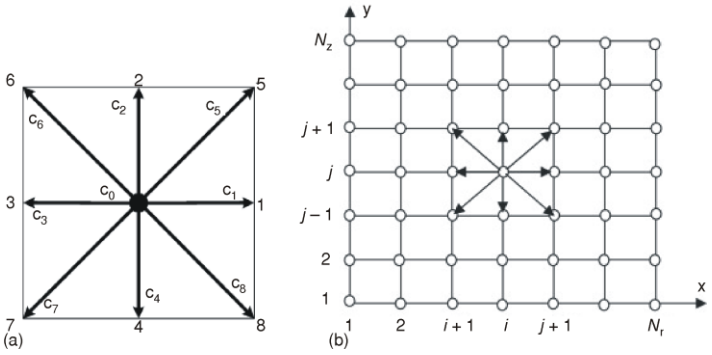

Figure 2. (a) Diagram of the D2Q9 lattice, (b) arrangement of lattices in a 2-D rectangular geometry

The nine velocities $\vec{c}_i$ and their corresponding weights ω_i in the D2Q9 lattice are the following:

$$c_0 = (0,0) \tag{31a}$$

$$\vec{c}_i = \left[\cos\left(\frac{i-1}{2}\pi\right), \quad \sin\left(\frac{i-1}{2}\pi\right)\right] C \text{ for } i = 1,2,3,4 \tag{31b}$$

$$\vec{c} = \sqrt{2}_i \left[\cos\left(\frac{2i-1}{4}\pi\right), \quad \sin\left(\frac{2i-1}{4}\pi\right)\right] C \text{ for } i = 5,6,7,8 \tag{31c}$$

$$C = \frac{\Delta x}{\Delta t} = \frac{\Delta y}{\Delta t} \tag{31d}$$

$$\omega_0 = \frac{4}{9}; \ \omega_{1,2,3,4} = \frac{1}{9}; \ \omega_{5,6,7,8} = \frac{1}{36} \tag{31e}$$

In case of heat transfer problems, the temperature is obtained after summing f_i over all direction [14], *i. e.*,

$$T(\vec{r},t) = \sum_{i=0}^{b} f_i(\vec{r},t) \tag{32a}$$

$$f_i^{(0)}(\vec{r},t) = \omega_i T(\vec{r},t) \tag{32b}$$

Equation (30), with definitions of temperature $T(\vec{r},t)$ and equilibrium function $f_i^{(0)}(\vec{r},t)$ given in eqs. (32a) and (32b) provide solution of a transient heat conduction problem without source term and within a Cartesian configuration in the LBM. To incorporate the volumetric radiation, eq. (30) gets modified to:

$$f_i(\vec{r}+\vec{c}_i\Delta t, t+\Delta t) = f_i(\vec{r},t) - \frac{\Delta t}{\tau}[f_i(\vec{r},t) - f_i^{(0)}(\vec{r},t)] - (\frac{\Delta t}{\rho c_p}) w_i \nabla \vec{q}_R(\vec{r},t) \tag{33}$$

The bounce-back scheme [14] is used in the current study for treating boundary conditions.

Results

Transient conduction and radiation heat transfer in a 2-D square enclosure is considered. In this, initially the entire system is at temperature $T_i = T_N = T_W = T_E$. For $t > 0$ the south boundary temperature is raised to $T_S = 2T$. The enclosed grey-homogeneous medium is absorbing, emitting and isotropically scattering. In the LBM-CVFEM, non-dimensional time step $\Delta x = 10^{-4}$(ξ = = $\alpha\beta 2t$) was considered and steady-state condition was assumed to have been achieved when the maximum variation in temperature at any location between two consecutive time levels did not exceed 10^{-5}. We investigate first the effect of LBM grid size on non-dimensional temperature T/T_s by comparing the steady-state (SS) results along the centreline $x/X = 0.5$ of the enclosure. Results obtained for aspect ratio $X/Y = 1$, extinction coefficient $\beta = 1.0$, scattering albedo $\omega = 0.5$, and conduction-radiation parameter $N = 0.1$, are listed in tab. 1.

Table 1. Effect of grid size in the LBM-CVFEM on steady state non-dimensional temperature at three locations, along the centerline $x/X = 0.5$

Resolution	$y/Y = 0.25$	$y/Y = 0.5$	$y/Y = 0.75$
8 × 8	0.88068	0.65539	0.61657
12 × 12	0.85569	0.67419	0.58855
16 × 16	0.82747	0.67315	0.58472
20 × 20	0.81809	0.66915	0.58130
25 × 25	0.81716	0.67275	0.58652

It is seen that on grids 20×20 and larger, the maximum variation in temperature is less than $5 \cdot 10^{-3}$. The trend observed with other sets of parameters was similar, and need not be reproduced here. It was decided to use 20×20 grids as basis for the subsequent computations. To facilitate the comparison of results, all further reported data were taken only at $x/X = 0.5$. They represent the normalized temperature T/T_s to the "south" wall, which is kept at temperature T_s as function of the normalized distance y/Y. Comparison of the LBM-CVFEM and the LBM-CDM [14] temperature results for the conduction-radiation parameter values $N = 0.01$, 0.1 and 1.0, is shown in fig. 3(a)-3(f). Results are obtained for an extinction coefficient $\beta = 1.0$, a scattering albedo $\omega = 0.0$ and black boundaries. It is seen from these figures that at all instants ξ, LBM-CVFEM and reference's results are in a good agreement. It can also be seen that at certain times, there is mismatch in the transient results of the two methods. This is in agreement with a general observation (tab. 2) that the LBM-CDM converges faster than the LBM-CVFEM to a steady-state (SS). In figs. 3(d)-3(f), extinction coefficient $\beta = 1.0$ and conduction radiation parameter $N = 0.01$, transient temperature

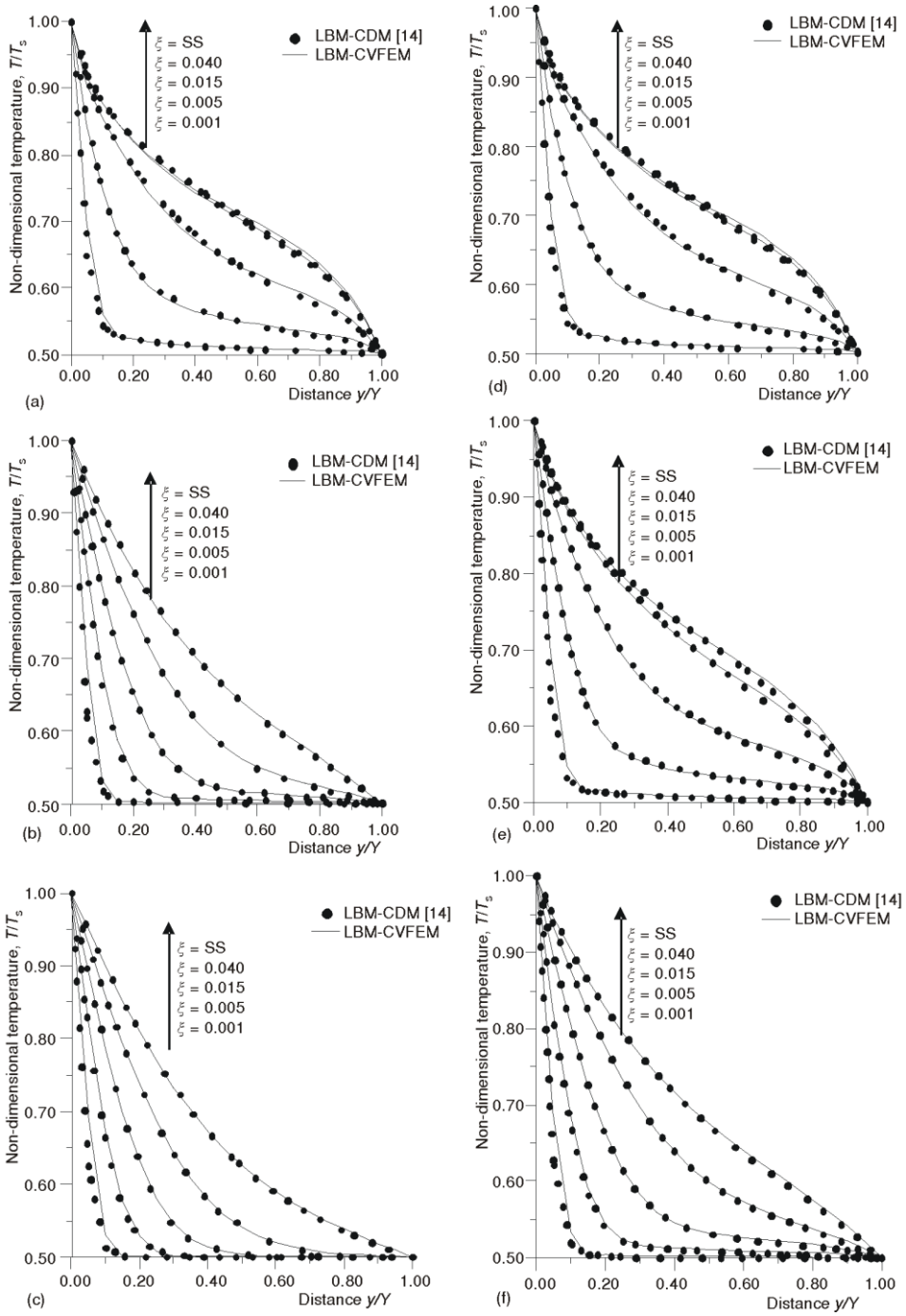

Figure. 3 Comparison of non-dimensional centerline temperature in a 2-D square enclosure at different instants ξ for (a) $N = 0.01$, (b) $N = 0.1$, (c) $N = 1.0$, (d) $\omega = 0.0$, (e) $\omega = 0.5$ and (f) $\omega = 0.9$

results of the LBM-CVFEM and the LBM-CDM are compared for two values of the scattering albedo $\omega = 0.5$ (scattering comparable to absorption fig. 3(e) and $\omega = 0.9$ – strong scattering fig. 3(f)). For the two cases, it can be seen that the results of the two methods agree very well. The LBM-CVFEM and the LBM-CDM numerical approaches are, also, compared in the case of a weakly participating medium ($\beta = 0.1$) and a good agreement is obtained (fig. 4).

Table 2. Comparison of the number of iterations required to obtain steady-state solutions with the LBM-CDM and the LBM-CVFEM for 20 × 20 control volumes/lattices

N	ω	LBM-CDM	LBM-CVFEM
0.01	0	642	670
0.01	0.5	823	886
0.01	0.9	1449	1593
0.1	0	1682	1772
1	0	1894	2078

The effect of the aspect ratio is illustrated in figs. 5(a)-5(b). In order to present it along with the effect of N and ω, only steady state results are presented. Two values of the aspect ratio are considered $X/Y = 1.0$ and $X/Y = 10.0$. For each value scattering and non scattering medium are tested and the calculation results show that the developed numerical approach predicts correctly the coupled conduction-radiation problems.

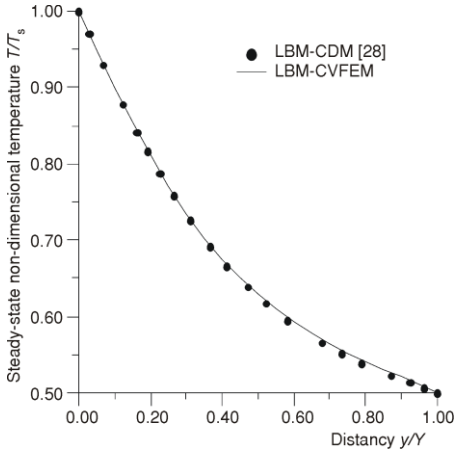

Figure 4. Comparison of steady state non-dimensional centerline temperature in a 2-D square enclosure for extinction coefficient $\beta = 0.1$

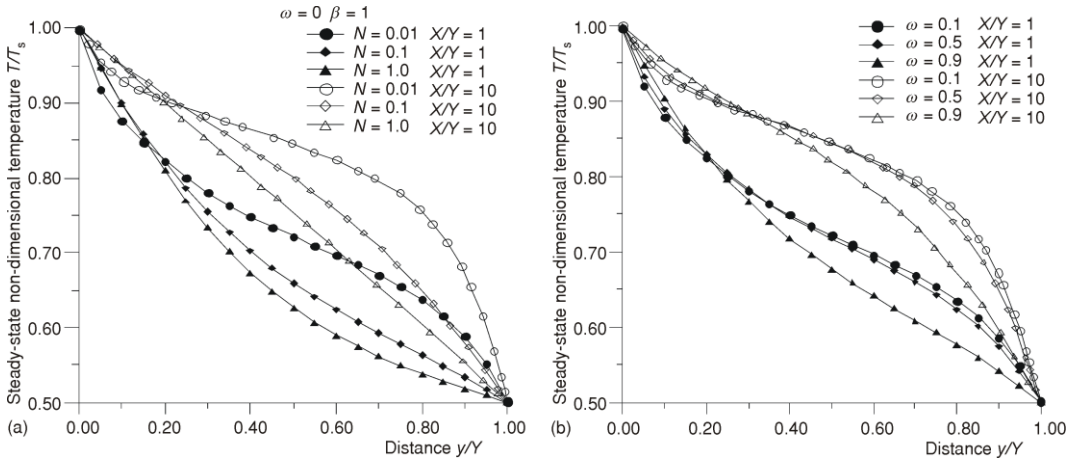

Figure 5. Steady state 2D LBM-CVFEM results for the non-dimensional centerline temperature (a) at aspect ratio $X/Y = 1.0$ and $X/Y = 10.0$ for different N, (b) at aspect ratio $X/Y = 1.0$ and $X/Y = 10.0$ for different ω

Conclusions

The lattice Boltzmann method (LBM) was used to solve the energy equation of transient conduction-radiation heat transfer problem in a 2-D square geometry containing an absorbing, emitting and scattering medium. Radiative source term in the energy equation was computed using the control volume finite element method (CVFEM). At our knowledge, the combination LBM-CVFEM is used for the first time to solve the conduction-radiation problems. In order to examine the accuracy and the computational efficiency of the proposed method, several test cases were investigated and obtained results were compared with those of the LBM-CDM (lattice Boltzmann method-Collapsed Dimension Method). For all cases, a good agreement was obtained and the two methods have a comparable number of iterations. On the other hand, the results presented here and the efficiency and robustness of LBM and CVFEM, allow the expectation that LBM-CVFEM will have advantages over conventional energy equation solvers, especially for problems with complex geometry.

Nomenclature

A^N – surface of the control volume ΔV_{ij}
b – number of directions in a lattice
$\vec{c}_i$ – velocity, [ms^{-1}]
c_p – specific heat capacity, [m^{2}s^{-1}K^{-1}]
f_i – particle distribution function, [K]
$f_i^{(0)}(\vec{r},t)$ – equilibrium function, [K]
G – incident radiation, [Wm^{-2}]
G_l – controids
I – radiative intensity, [Wm^{-2}sr^{-1}]
$I_b(s)$ – blackbody radiative intensity
i – direction
k – thermal conductivity, [Wm^{-1}K^{-1}]
k_a – absorption coefficient, [m^{-1}]
k_d – scattering coefficients, [m^{-1}]
N – conduction radiation parameter, [–]
$\vec{n}_w$ – unit normal vector on the wall
$\vec{q}_R$ – radiative heat [Wm^{-2}]
$\vec{r}$ – lattice node
$\Delta\vec{r}$ – lattice link
s – position, [m]
$T(\vec{r},t)$ – temperature, [K]
t – time, [s]
Δt – time step [s]
ΔV_{ij} – control volume, [m^3]
δV_{lij} – subvolume, [m^3]
x, y – Cartesian co-ordinates
Δx , Δy – regular steps

Greek symbols

β – extinction coefficient, [m^{-1}]
ε_w – wall emissivity
θ – polar angle, [rad]
ξ – dimensionless time, [–]
ρ – density, [kgm^{-3}]
σ – Stefan-Boltzmanconstant, [Wm^{-2}K^{-4}]
τ – relaxation time, [s]
Φ – scattering phase function $(\vec{\Omega}' - \Omega)$
$\Phi^{mnm'n'}$ – averaged scattering phase function
φ – azimuthal angle, [rad]
$\vec{\Omega}$ – outgoing direction of propagation
$\vec{\Omega}'$ – incoming direction
$\Delta\Omega^{mn}$ – control solid angle, [sr]
ω – scattering albedo, [–]
ω_i – weights in D2Q9 lattice

Subscripts

b – black body
W – wall index
ref – reference value

Superscripts

m,n,m′,n′ – indices for directions

References

[1] Succi, S., The Lattice Boltzmann Method for Fluid Dynamics and Beyond, *Oxford University Press*, Oxford, UK, 2001
[2] Higuera, F. J., *et al*., Lattice Gas Dynamics with Enhanced Collisions, *Europhys. Lett*, *9* (1989), 4, pp. 345-349
[3] Mohamed, A. A., *et al.*, Lattice Boltzmann Simulation of Natural Convection in an Open ended Cavity, *International Journal of Thermal Sciences*, *48* (2009), 10, pp. 1870-1875

[4] Benzi, R., *et al*, The Lattice Boltzmann Equation: Theory and Applications, *Phys. Rep*, *222* (1992), 3, pp. 145-197
[5] Semma, E., *et al*., Investigation of Flows in Solidification by using the Lattice Boltzmann Method, *International Journal of Thermal Science*, *47* (2008), 3, pp. 201-208
[6] Chen, S., Doolen, G. D., Lattice Boltzmann Method for Fluid Flows, *Ann. Rev. Fluid Mech*, *30* (1998), pp. 329-364
[7] He, X., *et al.*, A Novel Thermal Model for the Lattice Boltzmann Method in Incompressible Limit, *J. Comput. Phys*, *146* (1998), 1, pp. 282-300
[8] El Ganaoui, M., Djebali, R., Aptitude of a Lattice Boltzmann Method for Evaluating Transitional Thresholds for Low Prandtl Number Flows in Enclosures, *Comptes Rendus Mécanique*, *338* (2010), 2, pp. 85-96
[9] Wolf-Gladrow, D. A., Lattice Gas Cellular Automata and Lattice Boltzmann Models: An Introduction, Springer-Verlag, Berlin-Heidelberg, 2000
[10] Shan, X, Simulation of Rayleigh-Benard Convection using a Lattice Boltzmann Method, *Phys. Rev. E*, *55* (1977), 3, pp. 2780-2788
[11] Mezrhab, A. *et al.*, Hybrid Lattice-Boltzmann Finite-Difference Simulation of Convective Flows, *Comput. Fluids*, *33* (2005), 4, pp. 623-641
[12] El Ganaoui, M, Semma, E., A Lattice Boltzmann Coupled to Finite Volumes Method for Solving Phase Change Problems, *Thermal Science*, *13* (2009), 2, pp. 205-216
[13] Ho, J. R. *et al.*, Lattice Boltzmann Scheme for Hyperbolic Heat Conduction Equation, *Numer. Heat Transfer B*, *41* (2002), 6, pp. 591-607
[14] Meng, F., *et al*, Radiative Heat Transfer by the Discrete Transfer Method using an Unstructured Mesh, in: HTD-Vol. 244, *Radiative Heat Transfer: Theory and Applications*, *ASME* New York, USA, 1993, pp. 55-66
[15] Mishra, S. C., *et al*., Application of the Lattice Boltzmann Method for Solving the Energy Equation of a 2-D Transient Conduction-Radiation Problem, *International Journal of Heat and Mass Transfer*, *48* (2005), 17, pp. 3648-3659
[16] Chai, J. C., *et al.*, Evaluation of Spatial Differencing Practices for the Discrete-Ordinates Method. *J Thermophys Heat Transfer*, *8* (1994), 1, pp. 140-144
[17] Baek, S. W., Kim, M. Y., Analysis of Radiative Heating of a Rocket Plume Base with the Finite-Volume Method, *Int J Heat Mass Transfer*, *40* (1997), 7, pp. 1501-1508
[18] Rousse, D. R., Numerical Prediction of Two-Dimensional Conduction, Convection, and Radiation Heat Transfer. I - Formulation, *Int J Therm Sci*, *39* (2000), 3, pp. 315-331
[19] Rousse, D. R., Baliga, B. R., Formulation of a Control-Volume Finite Element Method for Radiative Transfer in Participating Media., *Proceedings*, 7th International Conference Num. Meth. Thermal Problems, Stanford University, Palo Alto, Cal., USA, 1991, pp. 786-795
[20] Rousse, D. R. *et al*, Numerical Prediction of Two-Dimensional Conduction, Convection, and Radiation Heat Transfer, II - Validation, *Int. J. Therm. Sci.*, *39* (2000), 3, pp. 332-353

Paper submitted: July 22, 2010
Paper revised: January 28, 2011
Paper accepted: February 24, 2011